Journal of Power Sources 251 (2014) 296–304

Contents lists available at ScienceDirect

Journal of Power Sources

journal homepage: www.elsevier.com/locate/jpowsour

$Li_3V_2(PO_4)_3$/C composite materials synthesized using the hydrothermal method with double-carbon sources

Chun-Chen Yang [a,b,*], Shu-Hsien Kung [a], S.J. Lin [b], Wen-Chen Chien [a]

[a] Department of Chemical Engineering, Ming Chi University of Technology, New Taipei City 243, Taiwan, ROC
[b] Battery Research Center of Green Energy, Ming Chi University of Technology, New Taipei City 243, Taiwan, ROC

HIGHLIGHTS

- LVP/C composites were prepared by a hydrothermal method and post-thermal treatment.
- Double carbon sources, i.e. PS sphere and carbon sphere, use on LVP/C.
- LVP/C composite showed excellent electrochemical performance.

GRAPHICAL ABSTRACT

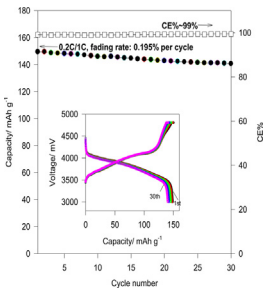

ARTICLE INFO

Article history:
Received 7 October 2013
Received in revised form
7 November 2013
Accepted 19 November 2013
Available online 1 December 2013

Keywords:
$Li_3V_2(PO_4)_3$/C composite
Cathode materials
Polystyrene (PS)
Carbon sphere (CS)
Li-ion batteries

ABSTRACT

This study presents the preparation of $Li_3V_2(PO_4)_3$/C composite material by using a hydrothermal method and post-thermal treatment. By adding a 5 wt.% polystyrene (PS) sphere and a 2 wt.% carbon sphere (CS) to the $Li_3V_2(PO_4)_3$/C composite material, the rate capability and cycle performance stability greatly improved. The characteristic properties of the $Li_3V_2(PO_4)_3$/C composite material were examined using X-ray diffraction (XRD), micro-Raman spectroscopy, scanning electron microscopy (SEM), an AC impedance method, and a galvanostatic charge–discharge method. For comparison, $Li_3V_2(PO_4)_3$/C composite material without CS fillers was also prepared. Thus, the $Li_3V_2(PO_4)_3$/C composite material with a 5% polystyrene sphere and a 2% CS displayed discharge capacities of 195, 171, 165, 158, 149, 140, and 90 mAh g^{-1} at rates of 0.1, 0.2, 0.5, 1, 3, 5, and 10 C, respectively. Even at a 1 C discharge rate for 30 cycles, the composite presented a capacity of 151–142 mAh g^{-1} and excellent cycling performance with a fading rate of 0.195% per cycle. The outstanding performance was attributed to the particular morphology and uniform carbon-layer coating of the $Li_3V_2(PO_4)_3$/C composite material, which proved to be a suitable candidate for application in Li-ion batteries.

1. Introduction

Lithium-ion batteries, because of their relatively high-energy capacity, are used in cell phones, laptop computers, digital cameras, renewable energy storage, electric vehicles (EVs), and smart grid applications. The $LiFePO_4$ cathode material proposed by Padhi et al. [1] has attracted extensive attention for application in next-generation rechargeable lithium-ion batteries because of low cost, environmental benignancy, excellent safety characteristics, high capacity (theoretical capacity ca. 170 mAh g^{-1}), and excellent cycling performance. However, the poor conductivity of the electron and ion transfer of lithium-ion batteries is a substantial barrier for commercial use. Compared with $LiFePO_4$ materials, monoclinic $Li_3V_2(PO_4)_3$ [2–31] cathode materials offer superior electrochemical properties, such as a high theoretical specific capacity of

* Corresponding author. Department of Chemical Engineering, Ming Chi University of Technology, New Taipei City 243, Taiwan, ROC.
E-mail address: ccyang@mail.mcut.edu.tw (C.-C. Yang).

0378-7753/$ – see front matter © 2013 Elsevier B.V. All rights reserved.
http://dx.doi.org/10.1016/j.jpowsour.2013.11.072

ca. 197 mAh g^{-1} and high potentials of 3.60, 3.65, and 4.10 V for V^{4+}/V^{3+} and 4.55 V for V^{5+}/V^{4+} [2,3]. Moreover, the lithium-ion diffusivity of monoclinic $Li_3V_2(PO_4)_3$ materials is 10^{-9}–10^{-10} cm^2 s^{-1}, which is much higher than that of $LiFePO_4$ materials at 10^{-14}–10^{-16} cm^2 s^{-1} [7]. However, regarding other polyanion materials, the separated (VO_6) octahedral in monoclinic material reduces electronic conductivity and results in a low rate capability performance. Three methods that improve electronic conductivity include the following: (1) carbon coating [5,14,15,17,23], (2) doping with supervalent cations [8,13,19,21,22,24], and (3) decreasing the particle size. Carbon coating is an effective and simple method for improving the electronic conductivity of $Li_3V_2(PO_4)_3$ materials. $Li_3V_2(PO_4)_3$ cathode materials can usually be prepared using a solid-state reaction [11–13], sol–gel process [25,29], spray-dried process [9,10], and hydrothermal process [18]. Previous studies [18] have revealed that high-quality crystalline $Li_3V_2(PO_4)_3$ material can be obtained using a hydrothermal process.

In this study, we prepared $Li_3V_2(PO_4)_3$/C composite materials by using a hydrothermal process and post-thermal process at temperatures of 750, 800, and 850 °C. Both a polystyrene (PS) polymer and a lab-made nanosized PS sphere (approximately 100 nm in size), as well as an aromatic structured polymer, were used as the carbon coating sources. In addition, the as-prepared nanosized carbon sphere (CS; ca. 300 nm) was also added as a conductive additive to improve electronic conductivity. The characteristic properties of $Li_3V_2(PO_4)_3$/C composite materials were examined using X-ray diffraction (XRD), micro-Raman spectroscopy, scanning electron microscopy (SEM), high-resolution transmission microscopy (HR-TEM), and elemental analysis (EA). The electrochemical performance of the $Li_3V_2(PO_4)_3$/Li cells were examined using a galvanostatic charge–discharge method, cyclic voltammetry, and AC impedance method.

2. Experimental

2.1. Preparation of $Li_3V_2(PO_4)_3$/C composite cathode materials

The $Li_3V_2(PO_4)_3$/C composite materials were prepared using a hydrothermal process and post-sintering process. Appropriate quantities of oxalic acid, NH_4VO_3, $LiOH.H_2O$, and $NH_4H_2PO_4$ (Aldrich) as the starting materials were dissolved in 200 mL deionized water. The molar ratio of Li:V:P was maintained at 3:2:3. The oxalic acid was used as a reducing agent that reduced V^{5+} to V^{3+}. The molar ratio of V:oxalic acid was 1:3. A suitable amount of adipic acid was used as a chelating agent in the study. The molar ratio of V:adipic acid was set at 1:1. The typical process involved can be described as follows: 50 mL of styrene monomer was added to 450 mL of deionized water, which was purged with nitrogen in advance. The mixture was then heated to 70 °C, and then 0.1 M $K_2S_2O_8$ was added to the mixture solution as an initiator. The mixture solution was maintained at 70 °C for 24 h under nitrogen. The as-prepared PS colloid was washed with ethanol and centrifuged at 10,000 rpm for 30 min to obtain 100-nm PS spheres. The CS was synthesized using a hydrothermal process with 8 wt.% glucose at 180 °C for 12 h [18,32]. The PS (MW 35,000, Aldrich) polymer was dissolved in acetyl acetate to form a 5-wt.% PS stock solution. The PS sphere was also added to a precursor solution. A suitable amount of PS sphere and CS was slowly added to the precursor solution mixture while stirring. The total carbon source for the $Li_3V_2(PO_4)_3$/C composite materials was maintained at 10 wt.%. The PS sphere was prepared using an emulsion polymerization method [33]. The mixed solution was transferred into a 600-mL Teflon-lined stainless steel autoclave, which was heated at 180 °C for 10 h. After the solution cooled to room temperature, the precipitate composite powder was cleaned and dried at 60 °C for 12 h in a vacuum oven, followed by post-sintering at 750 °C, 800 °C, and 850 °C for 10 h under an Ar/H_2 (95%:5%, v/v) atmosphere. The pure LVP cathode material was also prepared with the same condition without addition any carbon sources for comparison.

2.2. Material characterization

The crystal structure of the $Li_3V_2(PO_4)_3$/C composite samples was examined using an XRD spectrometer (Philips, X'pert Pro System). The surface morphology was conducted using an SEM (Hitachi 2600). The residue carbon morphology was observed using a HR-TEM (JEOL 2010F). The micro-Raman spectra were recorded on a confocal micro-Renishaw with a 632-nm He–Ne laser excitation. The residual carbon content in the samples was analyzed using an elemental analyzer (Perkin Elmer 2400). The electron conductivity of the composite samples was measured using the AC impedance method (AutoLab, Eco Chemi PGSTAT 30).

2.3. Electrochemical property measurements

The electrochemical performance of the Li/$Li_3V_2(PO_4)_3$ half cell was tested as a Li-ion half-cell using a CR 2032 coin cell (assembled in an argon-filled glovebox, Mbraun, Germany). The $Li_3V_2(PO_4)_3$/C composite electrodes were prepared by mixing active $Li_3V_2(PO_4)_3$/C materials, Super P, and poly (vinyl fluoride) (PVDF) binder in a weight ratio of 80:10:10, pasting the mixture on aluminum foil (Aldrich), and then drying the mixture in a vacuum oven at 120 °C for 12 h. Lithium foil (Aldrich) was used as the counter and reference electrode. A micro-porous PE film was used as the separator. The electrolyte was 1 M $LiPF_6$ in a mixture of EC and DEC (1:1 in v/v, Merck). The $Li_3V_2(PO_4)_3$/C composite batteries were charged by a constant current and a constant-voltage protocol (CC–CV) and discharged by a constant-current mode over a potential range of 3.0 V–4.8 V (vs. Li/Li^+) at varied C rates by using a battery tester (Arbin BT2000). The second CV charge step of 4.8 V was terminated when the charged current was below 0.1 C. The cyclic voltammetry (CV) was conducted using an AutoLab instrument at a scanning rate of 0.1 mV s^{-1} between 2.5 V and 4.3 V (vs. Li/Li^+). The AC impedance spectroscopy was used to obtain the AC spectra with an AutoLab PGSTAT302N potentiostat in a frequency range of 100 kHz to 10 mHz by applying 5 mV amplitude at open circuit potential (OCP). All tests were performed at room temperature.

3. Results and discussion

The XRD patterns of the $Li_3V_2(PO_4)_3$/C composite material, which used a 8%PS polymer as a carbon source and which was prepared using the hydrothermal method at 750 °C, 800 °C, and 850 °C, are presented in Fig. 1(a). Fig. 1(b) also shows the XRD patterns of the $Li_3V_2(PO_4)_3$/8%PS polymer, the $Li_3V_2(PO_4)_3$/5%PS sphere, and the $Li_3V_2(PO_4)_3$/5% PS sphere + 2% CS filler samples sintered at 800 °C for comparison. All XRD diffraction peaks for all of the samples are well-indexed as monoclinic $Li_3V_2(PO_4)_3$ materials with a space group of $P2_1/n$. The crystallinity of the $Li_3V_2(PO_4)_3$/C composite at 850 °C was much better than that of the $Li_3V_2(PO_4)_3$/C composites at 750 °C and 800 °C because the peaks at (020) and (121) of the sample calcined at 850 °C were much sharper and produced a stronger intensity. According to the structure refinement (TOPAS) results, the $Li_3V_2(PO_4)_3$/C composite materials with a 5% PS sphere plus a 2% CS exhibited lattice parameters with $a = 8.5757$ Å, $b = 8.6312$ Å, $c = 12.026$ Å, and $\beta = 90.58°$, which were consistent with the JCPD values listed in Table 1. In addition, the $Li_3V_2(PO_4)_3$/C cathode materials with an 8% PS polymer and a 5% PS sphere also exhibited the same lattice parameter values as listed in Table 1, indicating that these carbon sources had no observable

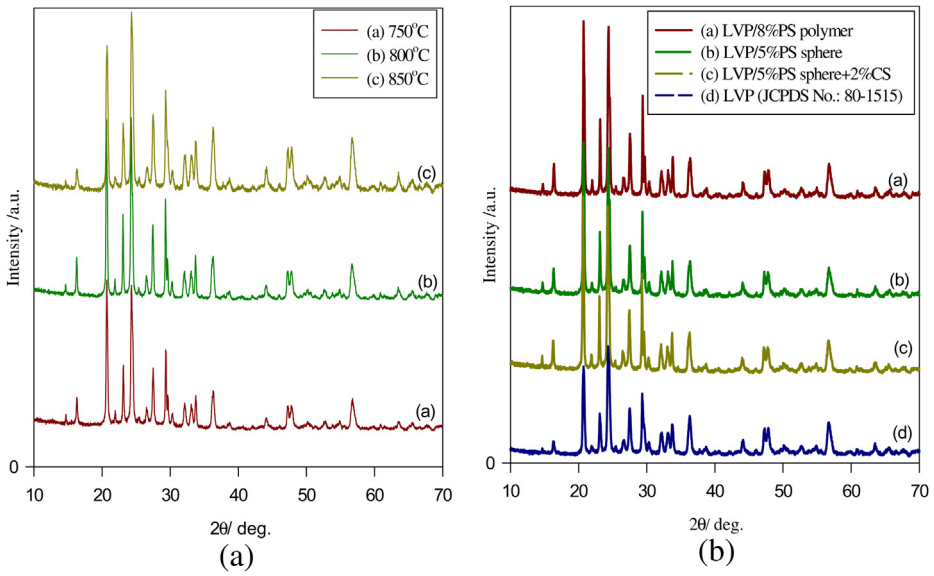

Fig. 1. (a) XRD patterns of $Li_3V_2(PO_4)_3$/8%PS polymer synthesized at temperatures of 750, 800, and 850 °C; (b). XRD patterns for the LVP/C samples with different carbon sources at 800 °C.

influence on the structure of $Li_3V_2(PO_4)_3$/C composite materials. The carbon was not observed on the XRD diffraction pattern, which indicated that the residual carbon was an amorphous structure or that the thickness of the carbon layer on the LVP was too thin to be detected. The added carbon source in the preparation process could prevent particle size growth. However, the residual carbon content was determined using elemental analysis (EA) in the composites displayed in Table 2. The residual carbon content of the $Li_3V_2(PO_4)_3$/C composite materials with an 8% PS polymer and a 5% PS sphere as the carbon sources was approximately 4.92%–4.94%; however, the $Li_3V_2(PO_4)_3$/C composite materials with a 5% PS sphere plus a 2% CS as the carbon source was 6.04%. Fig. 2 presents the SEM images of the $Li_3V_2(PO_4)_3$/C composites with various carbon sources. The $Li_3V_2(PO_4)_3$/C composite powder with an 8% PS polymer exhibited an irregular shape with some agglomeration. However, the $Li_3V_2(PO_4)_3$/C composite powder with a 5% PS sphere, 5% PS sphere, and 5% CS demonstrated a sharp 1D needle-like morphology exhibiting little agglomeration. The LVP powders with 1D morphology may be effective for electron transport and improving the rate capability. Fig. 3(a) shows the TEM image of the $Li_3V_2(PO_4)_3$/8%PS polymer sample. It was found that a non-uniform carbon coating on $Li_3V_2(PO_4)_3$/8%PS polymer sample with a thickness of approximately 2–10 nm was observed. In contrast, Fig. 3(b) presents the TEM image and selective area electron diffraction (SAED) pattern of the $Li_3V_2(PO_4)_3$/C composite powder with a 5% PS sphere and a 5% PS sphere plus a 2% CS. Regarding the results, a uniform carbon coating with a thickness of approximately 10 nm was observed on the LVP particle surface. The inset of Fig 3 displays the SAED pattern, indicating a well-crystallized structure and no other crystalline phases were presented except for the monoclinic $Li_3V_2(PO_4)_3$ phase.

Fig. 4 presents the micro-Raman spectra of the $Li_3V_2(PO_4)_3$/C composites with a 5% PS sphere and a 5% PS sphere plus a 2% CS in the range of 200–2000 cm^{-1}. In the spectra, two intense broad peaks at 1320 cm^{-1} and 1580 cm^{-1} were attributed to the disorder-induced phonon mode (D-band) and the graphite-like band (G-band), respectively. As presented in Table 3, the R_1 value ($=I_D/I_G$) of three $Li_3V_2(PO_4)_3$/C composites was approximately 1.0–1.10 and the R_2 value ($=(I_D + I_G)/I_{PO_4}$) varied significantly. The higher R_2 value was attributed to a more uniform carbon coating on the LVP particle surface. The $Li_3V_2(PO_4)_3$/C composites with a 5% PS sphere plus a 2% CS exhibited the highest R_2 value of approximately 3.283; by contrast, the $Li_3V_2(PO_4)_3$/C composites with an 8% PS polymer carbon source displayed the lowest R_2 value. This low R_2 value resulted from the low wetting ability of the PS polymer and low residual carbon content after sintering.

Fig. 5 presents the CV curves of three $Li_3V_2(PO_4)_3$/C composites with an 8% PS polymer, a 5% PS sphere, and a 5% PS sphere plus a 2%

Table 1
XRD parameters for varied $Li_3V_2(PO_4)_3$/C cathode materials.

Samples	Data				
	Parameters				
	a (Å)	*b* (Å)	*c* (Å)	Volume (Å^3)	Δ*V* (%)
$Li_3V_2(PO_4)_3$/C with 8%PS polymer	8.5625	8.6239	12.004	886.33	−0.00389
$Li_3V_2(PO_4)_3$/C with 5%PS sphere	8.5793	8.6253	12.003	888.24	−0.00174
$Li_3V_2(PO_4)_3$/C with 5%PS sphere+2%CS	8.5757	8.6312	12.026	890.12	0.000371
$Li_3V_2(PO_4)_3$ JCPDS No.:80-1515 data	8.6053	8.5912	12.362	889.79	–

Table 2
The carbon residual contents of $Li_3V_2(PO_4)_3$/C cathode materials.

Samples	Data				
	Sample#1		Sample#2		Average C/%
	Weight/mg	C/%	Weight/mg	C/%	
$Li_3V_2(PO_4)_3$/C with 8 wt.%PS polymer	2.022	4.91	1.832	4.92	4.92
$Li_3V_2(PO_4)_3$/C with 5 wt.%PS sphere	1.957	4.98	1.751	4.90	4.94
$Li_3V_2(PO_4)_3$/C with 5 wt.%PS sphere +2 wt.%CS	2.222	6.00	1.646	6.08	6.04

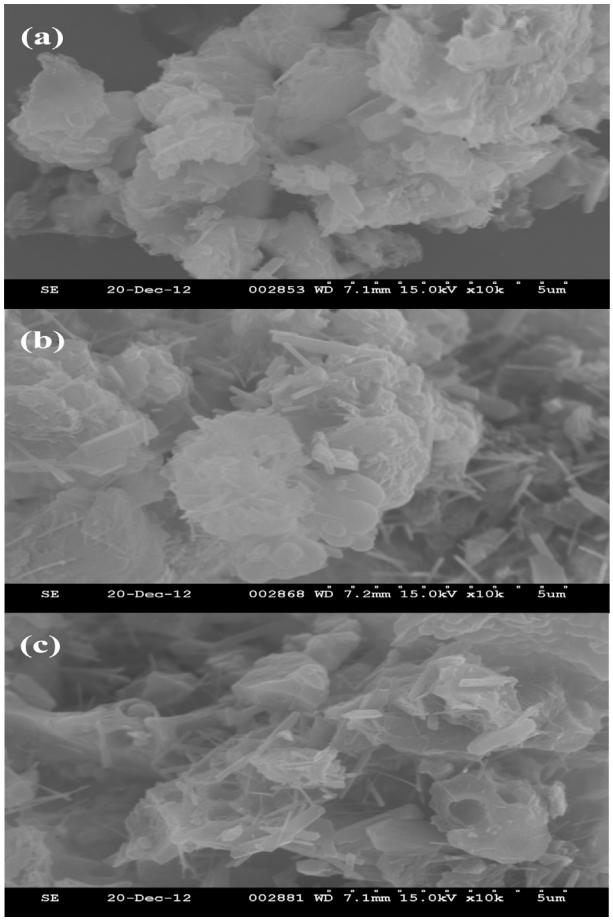

Fig. 2. SEM images of $Li_3V_2(PO_4)_3$/C with different carbon sources, (a) LVP/8 wt.%PS polymer; (b) LVP/5 wt.%PS sphere; (c) LVP/5 wt.%PS sphere/2 wt.%CS.

CS in the potential range of 3.0–4.3 V at a scan rate of 0.1 mV s^{-1} at 25 °C. As presented in Fig. 5, all three $Li_3V_2(PO_4)_3$/C composite electrodes presented three couples of oxidation (denoted as a'/a, b'/b, and c'/c) and reduction peaks between 3.0 and 4.3 V. Between the 3.0 and 4.3 V regions, the peak current intensity of the three $Li_3V_2(PO_4)_3$/C composite couples was markedly varied. Table 4 displays the peak potential positions (E_{pa}, E_{pc}), current intensity (i_{pa}, i_{pc}), potential differences (ΔE_1, ΔE_2, ΔE_3), and peak ratios (R_1, R_2, R_3) in detail for LVP/C composites using various types of carbon sources. By comparison, the pure $Li_3V_2(PO_4)_3$/C material demonstrated slow kinetics in the CV curve, indicating a broad peak and low current peak. This slow kinetics may be due to the low electron conductivity of LVP material. By contrast, the $Li_3V_2(PO_4)_3$/C composite with a 5 wt.% PS sphere as a carbon source exhibited good reaction kinetic and better reversibility properties, which were indicated by sharp oxidation and reduction current peaks and lower potential difference values (ΔE). However, the $Li_3V_2(PO_4)_3$/C composite with a 5 wt.% PS sphere plus a 2% CS carbon source exhibited the fastest reaction kinetic and excellent reversibility performance compared with the pure LVP and LVP/C composites with only a 5% PS sphere. The $Li_3V_2(PO_4)_3$/C composite with a 5 wt.% PS sphere plus a 2% CS carbon source also exhibited sharp and symmetric oxidation and reduction peaks and high current intensity. Overall, when a suitable amount of 3D CS fillers was added to the $Li_3V_2(PO_4)_3$/C composite, the electrochemical performance was greatly improved.

Fig. 6 displays the initial charge–discharge curves of the $Li_3V_2(PO_4)_3$/C composites with an 8% PS polymer, a 5% PS sphere, and a 5% PS sphere plus a 2% CS filler in the potential range of 3.0–4.8 V at a rate of 0.1 C. The three samples exhibited four voltage plateaus in the charge process at 3.69, 3.70, 4.10, and 4.55 V and four voltage plateaus in the discharge process at approximately 3.58, 3.65, 4.04, and 4.50 V. The potential plateau difference (ΔE) observed between the charge and the discharge of each pair of reactions was small, indicating the excellent reversibility of Li^+ extraction and insertion reactions for all $Li_3V_2(PO_4)_3$/C composites. The discharge capacity of the $Li_3V_2(PO_4)_3$/C composites with an 8% PS polymer was achieved at approximately 166.1 mAh g^{-1} at a rate of 0.1 C and, by contrast, at 167.2 mAh g^{-1} for the $Li_3V_2(PO_4)_3$/C composites with a 5% PS sphere. However, the $Li_3V_2(PO_4)_3$/C composite with a 5% PS sphere plus a 2% CS filler exhibited the highest discharge capacity of 194.1 mAh g^{-1} at 0.1 C (i.e., approximately 98.52% of theoretical capacity). The inset of Fig. 6 presents the cycling performance of the $Li_3V_2(PO_4)_3$/C composites with a 5% PS sphere plus a 2% CS carbon source at 0.1 C for 100 cycles. The initial discharge capacity was 190.01 mAh g^{-1} and more than 95.26% of the initial discharge capacity was maintained after 100 cycles (at a fading rate of approximately 4.7%). When we tested at charge/discharge rates of 0.2/0.2 C, 0.2/0.5 C, 0.2/1 C, 0.2/3 C, and 0.2/5 C, the $Li_3V_2(PO_4)_3$/C composite material with a 5% PS sphere plus a 2% CS filler exhibited the discharge capacities of 195, 171, 165, 158, 149, 140, and 90 mAh g^{-1} at rates of 0.1, 0.2, 0.5, 1, 3, 5, and 10 C, respectively, as shown in Fig. 7.

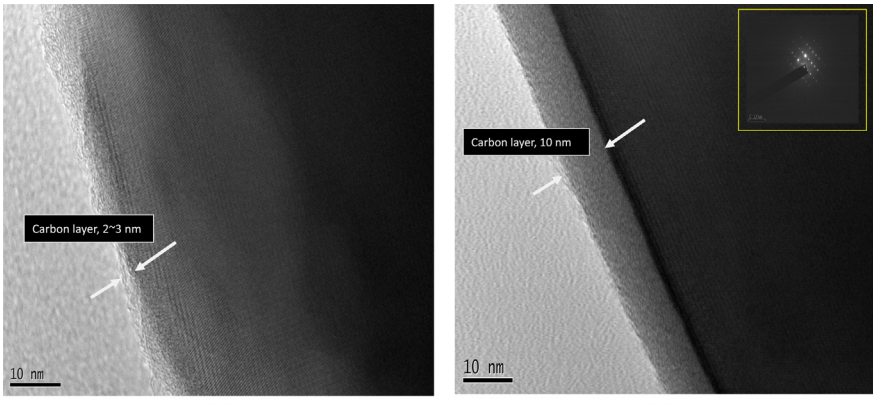

Fig. 3. (a). TEM image for LVP/8%PS polymer sample; (b). TEM image of synthesized LVP/5%PS sphere + 2%CS sample material, the inset is SAED pattern.

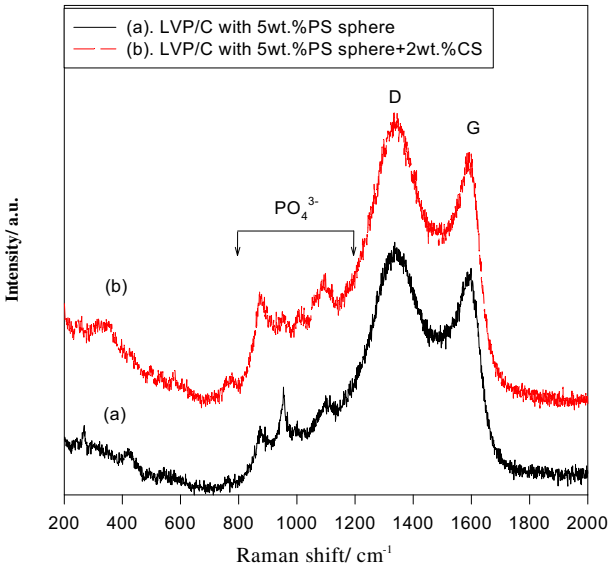

Fig. 4. Micro-Raman spectra of $Li_3V_2(PO_4)_3$/C with different carbon sources.

However, the discharge capacities of the $Li_3V_2(PO_4)_3$/C composites with an 8% PS polymer at charge/discharge rates of 0.2/0.2, 0.2/0.5, 0.2/1, 0.2/3, and 0.2/5 C were 137.50, 133.50, 126.11, 95.10, and 60.45 mAh g^{-1}, respectively. Moreover, the discharge capacities of the $Li_3V_2(PO_4)_3$/C composites with only a 5% PS sphere at charge/discharge rates of 0.2/0.2, 0.2/0.5, 0.2/1, 0.2/3, and 0.2/5 C rates are 165.26, 157.72, 147.06, 90.49, and 35.66 mAh g^{-1}, respectively. Apparently, the $Li_3V_2(PO_4)_3$/C composites with a 5% PS sphere plus a 2% CS filler demonstrated the highest electrochemical performance among the three LVP/C composites. For comparison, a few studies have reported the electrochemical performance of the $Li_3V_2(PO_4)_3$/C composites using the hydrothermal method [34,35]. Chang et al. [34] studied the carbon coated LVP composites using a hydrothermal method with a single carbon source (glucose). The study reported the initial discharge capacities of 178, 173, and 172 mAh g^{-1} at 0.1, 0.2, and 0.5 C, respectively, between 3.0 and 4.8 V. Teng et al. [35] also prepared LVP/C composites by using a hydrothermal method. They also used 20 wt.% glucose as a carbon source. The synthesized powder displayed plate-like morphology. The initial discharge capacity of LVP/C was 175.4 mAh g^{-1} at 0.1 C. After 100 cycles, the discharge capacity dropped to 140.7 mAh g^{-1} with a capacity retention of 80.2%. However, our sample presented a stable cycling performance rate of 0.1 C. The capacity retention (95.26%) was excellent over the first 100 cycles.

Fig. 8(a) and (b) presents the SEM images of the PS sphere and CS fillers, respectively. The PS carbon source and CS particle fillers exhibit nanosized dimensions and 3D needle-shaped morphology. It has a synergistic effect using those carbon sources. Generally, conventional carbon sources like glucose or sucrose are used instead of a PS sphere. Another advantage of the as-prepared PS sphere is its hydrophilic property, which is ideal for the hydrothermal process. The conventional carbon fillers were Super P carbon black, acetylene black, CNTs, graphene, and carbon nanofibers (CNFs). The 1D or 2D carbon fillers easily form aggregates with poor dispersion. By contrast, we propose using a 3D polymer carbon source (ca. 100-nm sphere) and 3D structure of CS fillers (ca. 200–500 nm). These fillers can reduce the aggregation problem of particles and maintain excellent particle dispersion in the LVP matrix.

Fig. 9 presents the rate capability performance of the $Li_3V_2(PO_4)_3$/C composites based on three types of carbon sources at various rates from 0.1 to 10 C. By comparison, the rate capability performance of the $Li_3V_2(PO_4)_3$/C composite with a 5% PS sphere plus a 2% CS filler was superior to that of the $Li_3V_2(PO_4)_3$/C composite with an 8% PS polymer and a 5% PS sphere. As presented in Fig. 9, the discharge capacities of the $Li_3V_2(PO_4)_3$/C composites were 195, 171, 165, 158, 149, 140, and 90 mAh g^{-1} at 0.1, 0.2, 0.5, 1, 3, 5, and 10 C, respectively. Table 5 lists the discharge capacities and current efficiency values at varied discharge rates for comparison. The high rate capability performance of the three $Li_3V_2(PO_4)_3$/C composites must be further improved although they display promising discharge capacities at a rate of 10 C. The optimal amounts of CS fillers must be adjusted to satisfy the high rate capability performance for future use on EV.

The AC impedance spectroscopy was used to investigate the interface properties of $Li_3V_2(PO_4)_3$/C composite samples. The AC spectra of the $Li_3V_2(PO_4)_3$/8%PS polymer, $Li_3V_2(PO_4)_3$/5%PS sphere, $Li_3V_2(PO_4)_3$/5% PS sphere + 2% CS samples at open circuit potential are illustrated in Fig. 10. Each AC plot consisted of one semicircle at a higher frequency followed by a linear portion at a lower frequency. The lower frequency region of the straight line was considered as the Warburg impedance, which was used for long-range lithium-ion diffusion in the bulk phase. R_b indicates the bulk resistance at the electrolyte, R_{ct} refers to the charge transfer resistance at the active material interface, and CPE represents the double-layer capacitance and surface film capacitances. The lithium chemical diffusion coefficients of the electrode were calculated based on Equation (1) [11–13]:

$$D_i = \frac{1}{2}\left(\frac{RT}{AF^2\sigma C}\right)^2 \quad (1)$$

where σ refers to the Warburg impedance coefficient (obtained by a slope from plot of Z_{re} vs.$\omega^{-0.5}$, as illustrated in the inset of Fig 10), D_{Li} to the lithium diffusion coefficient, R to the gas constant, T to the absolute temperature, F to Faraday's constant, A to the area of the electrode, and C to the molar concentration of Li^+ ions ($C_{Li} = 1.0 \times 10^{-3}$ mol cm^{-3}). Table 6 summarizes the calculated R_s, R_{ct}, D_i, and j_o parameters for three LVP/C composite samples. The R_s values of the $Li_3V_2(PO_4)_3$/8%PS polymer, $Li_3V_2(PO_4)_3$/5%PS sphere, $Li_3V_2(PO_4)_3$/5%PS sphere + 2% CS samples were approximately 8, 5.5 and 3.33 Ω, respectively. The values of R_{ct} and D_i for these three composite samples were greatly varied. After adding CS and the carbon coating, the charge resistance (R_{ct}) values and lithium diffusion coefficients (D_{Li}) were effectively improved, thereby enhancing the rate capability of LVP/C materials. The j_o value indicates the reaction kinetic of the LVP/C composite materials and can be obtained as follows: $j_o = RT/nFR_{ct}$. For comparison, we observed that the LVP/8%PS polymer sample exhibited an R_{ct} value of 262 Ω, a D_{Li} of 6.98×10^{-12} cm^2 s^{-1}, and a j_o value of ca. 9.80×10^{-5} A cm^{-2}; moreover, it was found that the LVP/5%PS sphere sample exhibited an R_{ct} value of 125 Ω, a D_{Li} of 3.79×10^{-12} cm^2 s^{-1}, and a j_o value of ca. 2.05×10^{-4} A cm^{-2}. By comparison, the LVP/C composite with a 5% PS sphere plus a 2% CS sample exhibited a much lower R_{ct} value of 57 Ω, a higher D_{Li} of 1.15×10^{-11} cm^2 s^{-1}, and also a higher j_o of ca. 4.50×10^{-4} A cm^{-2}. After the PS sphere and CS carbon fillers were added to the LVP/C composite material, both the electrochemical and rate capability performance were greatly enhanced. Wang et al. [36] reported that the lithium diffusion coefficient values of the LVP/C and LVP/LTO/C samples were $6–7 \times 10^{-11}$ cm^2 s^{-1} and $4–5 \times 10^{-10}$ cm^2 s^{-1}, respectively. Zhong et al. [37] also reported that the lithium diffusion coefficient values of LFP/C and 9LVP.LFP/C were 2.53×10^{-11} cm^2 s^{-1} and 1.88×10^{-10} cm^2 s^{-1}, respectively. Our lithium diffusion coefficient value (1.15×10^{-11} cm^2 s^{-1}) was of the same magnitude order as that of Zhong et al.

Table 3
The AC impedance results for varied $Li_3V_2(PO_4)_3$/C cathode materials.

Samples	Parameters				
	I_D (intensity/a.u.)	I_G (intensity/a.u.)	PO_4^{3-} (intensity/a.u.)	$R_1 = I_D/I_G$	$R_2 = (I_D + I_G)/PO_4^{3-}$
$Li_3V_2(PO_4)_3$/C with 8 wt.%PS polymer	2623.51	2490.15	2784.26	1.054	1.837
$Li_3V_2(PO_4)_3$/C with 5 wt.%PS sphere	2934.52	2664.16	2600.01	1.101	2.153
$Li_3V_2(PO_4)_3$/C with 5 wt.%PS sphere/2 wt.%carbon sphere	3938.28	3645.95	2310.4	1.080	3.283

Fig. 11 presents the cycling performance of the LVP/C composite material with a 5% PS sphere plus a 2% CS filler at 0.2 C charge and 1 C discharge rates during a 30-cycle test. The LVP/C sample exhibited excellent cycling stability with the discharge capacity of from 151 mAh g^{-1} to 142 mAh g^{-1} at 1 C. The capacity retention was ca. 95% and the fading rate was approximately 0.195% per cycle. The current efficiency result was excellent and maintained at 99%. The inset of Fig. 11 displays the charge/discharge curves of the LVP/C sample during the 30-cycle test. The results indicated a stable and excellent cycling performance. Chang et al. [34] also reported a high rate performance. Their study presented the discharge capacities of 136, 132, 127 mAh g^{-1} at 1, 2, and 5 C, respectively, between 3.0 and 4.8 V. Teng et al. [35] presented the discharge capacities of LVP/C at 172.8, 164.6, 155.7, 147, and 128 mAh g^{-1} at rates of 0.2, 0.6, 1.2, 2.5, and 6 C, respectively. When cycled at a rate of 1 C, the initial discharge capacity of 157.3 mAh g^{-1} dropped to 133.7 mAh g^{-1} after 200 cycles, with a capacity retention of 85%. The capacity fading may have been due to electrolyte oxidation and a significant overpotential in the high potential window. Clearly, both of these LVP/C samples exhibited lower rate capabilities than those in our study did. In short, the electrochemical performances of the LVP/C composite samples are highly dependent on the carbon content and uniformity. It was found that the carbon contents of our LVP/C samples are approximately 5–6%. The LVP/5%PS sphere + 2% CS sample shows slightly higher carbon content (ca. 6%), as compared with the LVP/8%PS polymer (4.92%) and LVP/5%PS sphere (4.94%) samples. The main reason may be due to the excellent uniformity of coated carbon layer for the LVP/5%PS sphere + 2%CS sample, as seen in Fig. 3(b). It was found that the LVP/8%PS polymer sample shows very poor carbon uniformity, as compared with the LVP/5%PS sphere + 2%CS sample, as shown in Fig. 3(a). Moreover, the LVP/5% PS sphere sample owns the 1D needle-like morphology, as seen in Fig. 2(b); it is good for the electron transport. Also, the PS sphere as the carbon sources in LVP/5%PS sphere composite sample is able to create many micro-pores at inside active materials. Clearly, those micro-pores are good for electrolyte uptake and lithium ion transport. Furthermore, the LVP/5%PS sphere + 2%CS sample also shows the 1D needle-like morphology with 3D nano-sized carbon fillers, as seen in Fig. 2(c), the electron transport can also be greatly enhanced. It is due to the 3D nano-sized carbon spheres can help to establish some fast electron transport channels in LVP/C powders. With the same reason on the LVP/5%PS sphere + 2%CS sample, there are many micropores in the composite as the electrolyte micro-reservoir. As a result, we have found that the LVP/5%PS sphere + 2%CS sample exhibits the best electrochemical performance, as compared with the other two samples.

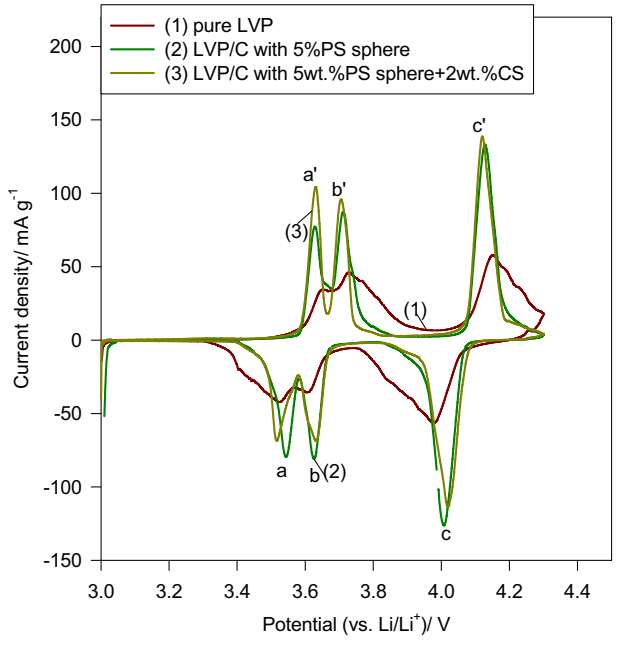

Fig. 5. Cyclic voltammograms of $Li_3V_2(PO_4)_3$/C composites with different types of carbon sources at a scan rate of 0.1 mV s^{-1} (3.0–4.3 V).

4. Conclusion

The hydrothermal method was applied to synthesize the $Li_3V_2(PO_4)_3$/C composite materials. The PS polymer, PS sphere, and CS carbon were used as the carbon sources and fillers. The optimal residual carbon content was examined at approximately 6.0% when the carbon source was a 5 wt.% PS sphere plus a 2% CS filler. The micro-Raman results also indicated that the *R* ratios were approximately 1.0–1.1, indicating high-quality carbon coating on the LVP particle with a uniform thickness of 10 nm. The results indicated that the discharge capacity of the $Li_3V_2(PO_4)_3$/C composite material with a 5-wt.% PS sphere plus a 2% CS carbon source were as high as 195 mAh g^{-1} and 90 mAh g^{-1} at 0.1 and 10 C, respectively. The

Table 4
CV parameters for $Li_3V_2(PO_4)_3$/C composites at 0.1 mV s^{-1}.

Para.	Data.		
	Pure LVP	LVP/5%PS sphere	LVP/5 wt.%PS sphere + 2%CS
$E_{p.a1}$/V	3.63	3.65	3.63
$E_{p.c1}$/V	3.54	3.52	3.52
ΔE_1/V	0.09	0.13	0.11
$i_{p.a1}$/mA cm^{-2}	77.27	34.45	104.25
$i_{p.c1}$/mA cm^{-2}	−79.46	−42.19	−68.57
$R_1(=i_{p.a1}/i_{p.c1})$	0.97	0.82	1.52
$E_{p.a2}$/V	3.71	3.73	3.71
$E_{p.a2}$/V	3.63	3.60	3.63
ΔE_2/V	0.08	0.13	0.08
$i_{p.a2}$/mA cm^{-2}	87.19	46.18	95.97
$i_{p.c2}$/mA cm^{-2}	−80.76	−35.65	−68.52
$R_2(=i_{p.a2}/i_{p.c2})$	1.08	1.30	1.46
$E_{p.a3}$/V	4.13	4.15	4.12
$E_{p.c3}$/V	4.01	3.98	4.02
ΔE_3/V	0.12	0.17	0.10
$i_{p.a3}$/mA cm^{-2}	133.23	58.01	138.92
$i_{p.c3}$/mA cm^{-2}	−126.17	−56.26	−113.45
$R_3(=i_{p.a3}/i_{p.c3})$	1.06	1.03	1.22

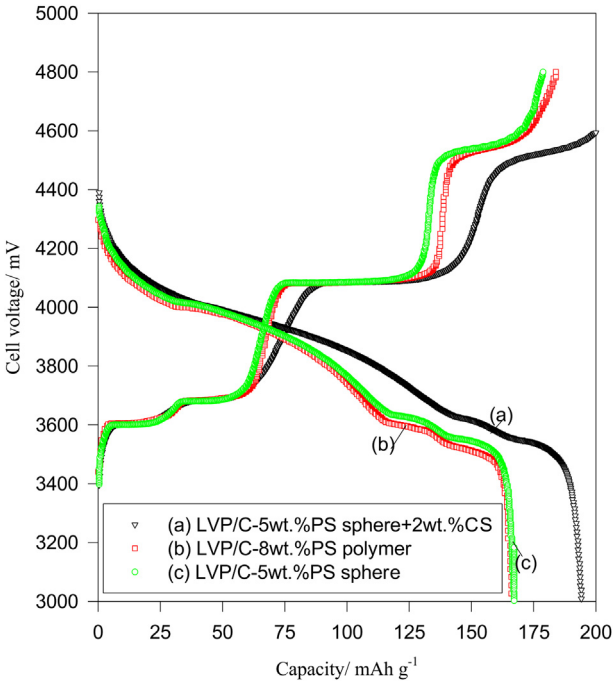

Fig. 6. The initial charge–discharge curves of $Li_3V_2(PO_4)_3$/C with different carbon sources at 0.1 C rate between 3.0 and 4.8 V.

discharge capacity of 19 mAh g^{-1} was approximately 98.4% of the theoretical capacity of LVP. The electrochemical performance of the $Li_3V_2(PO_4)_3$/C composites with a 5% PS sphere plus a 2% CS carbon filler was higher than that of the $Li_3V_2(PO_4)_3$/C composites with an 8% PS polymer and only a 5% PS sphere. The fading rate of the $Li_3V_2(PO_4)_3$/C composites with a 5% PS sphere plus a 2% CS carbon filler was only 0.195% per cycle, and the current efficiency was approximately 99% at a 0.2 C charge and 1 C discharge rates. The

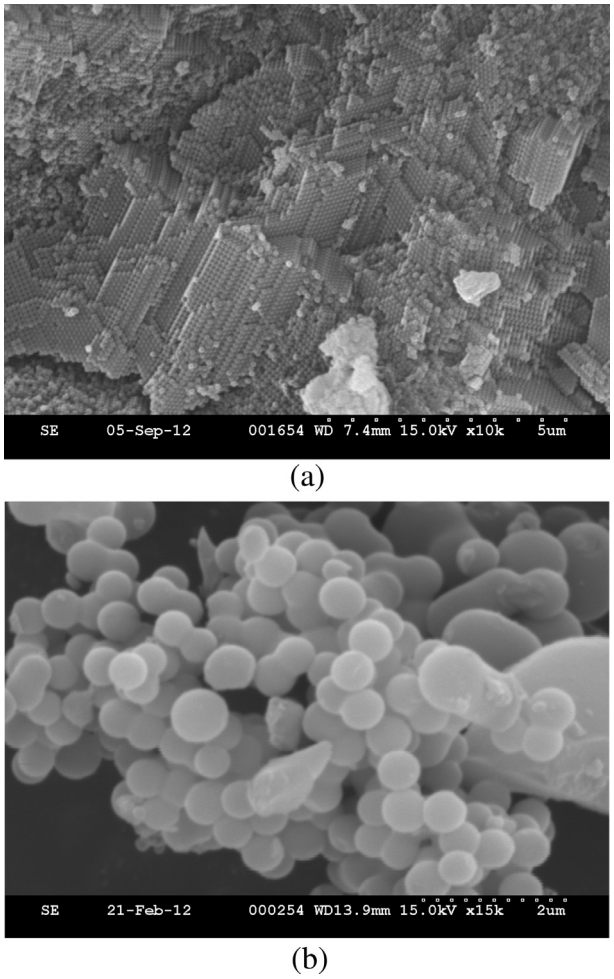

Fig. 8. SEM images: (a) polystyrene (PS) sphere; (b) carbon sphere (CS).

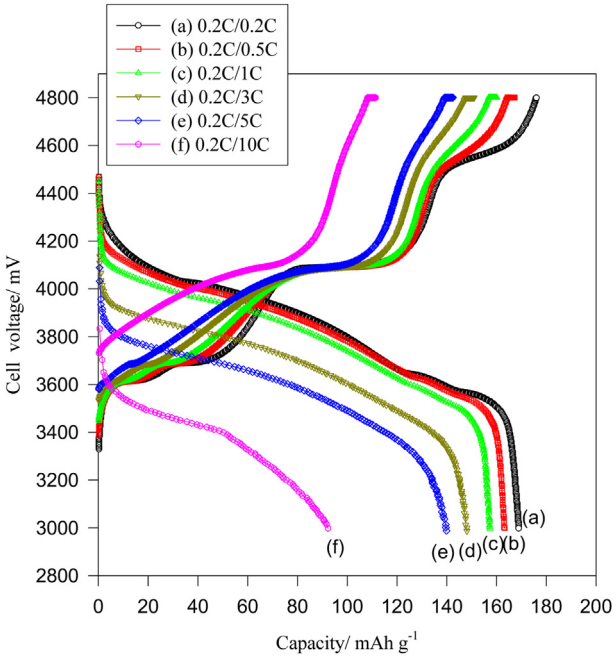

Fig. 7. The charge–discharge curve of $Li_3V_2(PO_4)_3$/C with different carbon sources at various C-rates (from 0.2 to 10 C) in the voltage of window of 3.0–4.8 V.

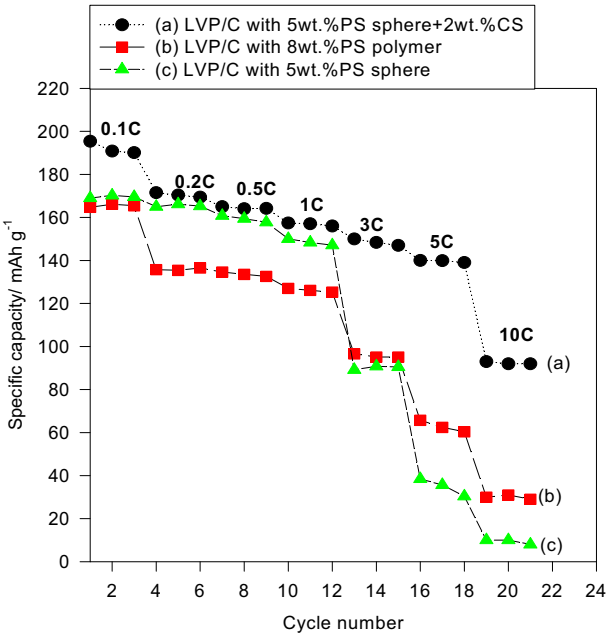

Fig. 9. The rate capabilities of $Li_3V_2(PO_4)_3$/C composites with different carbon sources at various C-rates, i.e., at 0.1C–10 C.

Table 5
The discharge capacities of LVP/C cathode at 0.2 C–10 C rate.

Item	Rate					
	0.2 C	0.5 C	1 C	3 C	5 C	10 C
Discharge capacity/mAh g^{-1}	171.5	163.3	157.4	148.1	139.9	92.3
Current efficiency/%	84.09	97.62	98.34	98.06	98.13	78.56

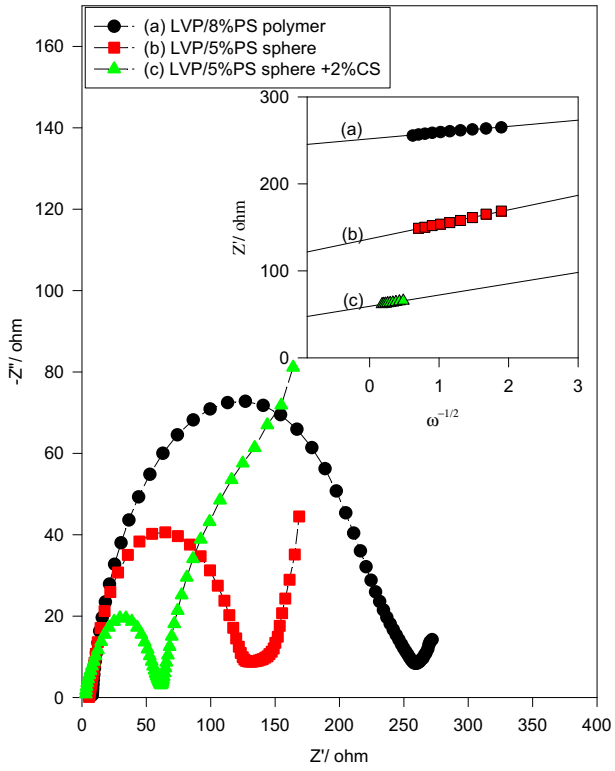

Fig. 10. The Nyquist plot of $Li_3V_2(PO_4)_3$/C with different carbon sources at OCP; the inset the relationship between Z′ and the inverse square root of frequency ($\omega^{-1/2}$) in the frequency range.

$Li_3V_2(PO_4)_3$/C composites exhibited excellent high-rate electrochemical performance by using double-carbon sources. These high electrochemical performance rates may be due to the carbon residual nanosized pores or void formation (PS sphere effect), favorable electron conduction channels (CS effect) in the matrix, uniform carbon-coating layer, and the particular needle-shaped morphology. It has a synergistic effect on $Li_3V_2(PO_4)_3$/C composites by using double-carbon sources.

Table 6
Lithium chemical diffusivities and exchange current densities of $Li_3V_2(PO_4)_3$/C composites.

Samples	Param.				
	R_s/Ω	R_{ct}/Ω	σ	$D_{Li}/cm^2\ s^{-1}$	$J_o/A\ cm^{-2}$
$Li_3V_2(PO_4)_3$/C with 8%PS polymer	8.0	262	16.69	6.98×10^{-12}	9.80×10^{-5}
$Li_3V_2(PO_4)_3$/C with 5%PS sphere	5.5	125	12.98	3.79×10^{-12}	2.05×10^{-4}
$Li_3V_2(PO_4)_3$/C with 5%PS sphere + 2%CS	3.33	57	7.16	1.15×10^{-11}	4.50×10^{-4}

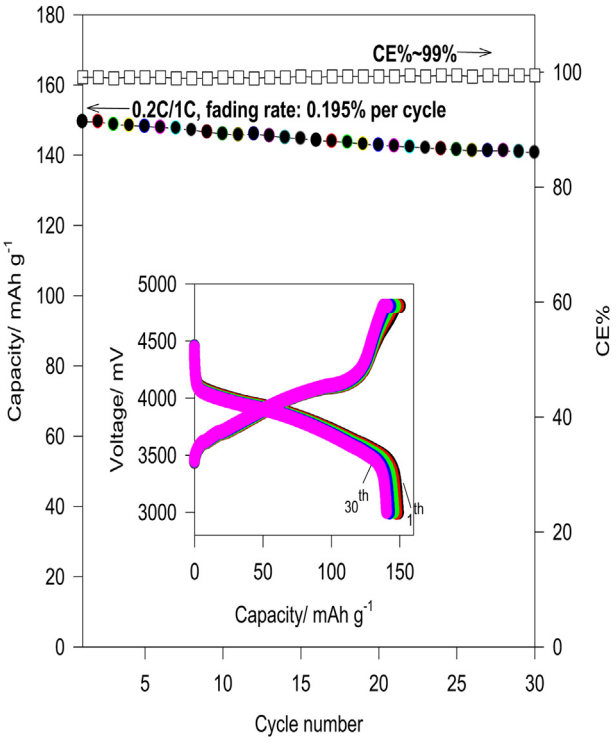

Fig. 11. The cycle performance of LVP/C cathode at 0.2 C/1 C rate.

Acknowledgments

Financial support from the National Science Council, Taiwan (Project No: NSC 101-2221-E-131-037) is gratefully acknowledged.

References

[1] A.K. Padhi, K.S. Nanjundaswamy, J.B. Goodenough, J. Electrochem. Soc. 144 (1997) 1188–1194.
[2] S.C. Yin, H. Grondet, L.F. Nazar, J. Am. Chem. Soc. 34 (2003) 10402–10411.
[3] D. Morgan, G. Ceder, M.Y. Saidi, J. Chem. Mater 11 (2002) 4684–4693.
[4] M. Morcrette, J.B. Leriche, C. Masquelier, Electrochem. Solid-State Lett. 5 (2003) A80–A84.
[5] H. Huang, S.C. Yin, T. Kerr, Adv. Mater. 14 (2002) 1525–1528.
[6] S.C. Yin, H. Grondey, P. Strobel, J. Am. Chem. Soc. 2 (2003) 326–327.
[7] S.C. Yin, P. Strobel, H. Grondey, Chem. Mater. 8 (2004) 1456–1465.
[8] J. Yao, S. Wei, P. Zhang, C. Shen, K. Aguey-Zinsou, L. Wang, J. Alloys Compd. 532 (2012) 49–54.
[9] Y. Jiang, W. Xu, D. Chen, Z. Jian, H. Zhang, Q. Ma, X. Cai, B. Zhao, Y. Chu, Electrochim. Acta 85 (2012) 377–383.
[10] B. Huang, X. Fan, X. Zheng, M. Lu, J. Alloys Compd. 509 (2011) 4765–4768.
[11] Y.Q. Qiao, J.P. Tu, X.L. Wang, C.D. Gu, J. Power Sources 199 (2012) 287–292.
[12] Y.Q. Qiao, X.L. Wang, Y.J. Mai, J.Y. Xiang, D. Zhang, C.D. Gu, J.P. Tu, J. Power Sources 196 (2011) 8706–8709.
[13] H. Liu, S. Bi, G. Wen, X. Teng, P. Gao, Z. Ni, Y. Zhu, F. Zhang, J. Alloys Compd. 543 (2012) 99–104.
[14] L. Ge, C. Han, L. Ni, J. Zhang, Y. Tao, Q. Yu, Y. Shen, A. Xie, L. Zhu, Y. Zhang, Solid State Sci. 14 (2012) 864–869.
[15] Q. Kung, Y. Zhao, J. Power Sources 216 (2012) 33–35.
[16] Z. Chen, C. Dai, G. Wu, M. Nelson, X. Hu, R. Zhang, J. Liu, J. Xia, Electrochim. Acta 55 (2012) 8595–8599.
[17] J. Yan, W. Yuan, Z.Y. Tang, H. Xie, W.F. Mao, L. Ma, J. Power Sources 209 (2012) 251–256.
[18] H. Liu, C. Cheng, X. Huang, J. Li, Electrochim. Acta 55 (2012) 8461–8465.
[19] Q. Kuang, Y. Zhao, X. An, J. Liu, Y. Dong, L. Chen, Electrochim. Acta 55 (2010) 1575–1581.
[20] Y.Q. Qiao, X.L. Wang, J.Y. Xiang, D. Zhang, W.L. Liu, J.P. Tu, Electrochim. Acta 56 (2011) 2269–2275.
[21] C. Dai, Z. Chen, H. Jin, X. Hu, J. Power Sources 195 (2010) 5775–5779.
[22] Y. Chen, Y. Zhao, X. An, J. Liu, Y. Dong, L. Chen, Electrochim. Acta 54 (2009) 5844–5850.
[23] Y.Q. Qiao, X.L. Wang, Y. Zhou, J.Y. Xiang, D. Zhang, S.J. Shi, J.P. Tu, Electrochim. Acta 56 (2010) 510–516.

[24] J.S. Huang, L. Yang, K.Y. Liu, Y.F. Tang, J. Power Sources 195 (2010) 5013–5018.
[25] Y. Li, Z. Zhou, X. Gao, J. Yuan, Electrochim. Acta 52 (2007) 4922–4926.
[26] X.H. Rui, N. Ding, J. Liu, C. Li, C.H. Chen, Electrochim. Acta 55 (2010) 2384–2390.
[27] M.Y. Saidi, J. Barker, H. Huang, J.L. Swoyer, G. Adamson, J. Power Sources 119–121 (2003) 266–272.
[28] J. Wang, J. Liu, G. Yang, X. Zhang, X. Yan, X. Pan, R. Wang, Electrochim. Acta 54 (2009) 6451–6454.
[29] J. Yan, W. Yuan, H. Xie, Z.Y. Tang, W.F. Mao, L. Ma, Mater. Lett. 71 (2012) 1–3.
[30] A. Pan, J. Liu, J.G. Zhang, W. Xu, G. Cao, Z. Nie, B.W. Arey, S. Liang, Electrochem. Commun. 12 (2010) 1674–1677.
[31] A. Tang, X. Wang, G. Xu, R. Peng, H. Nie, Mater. Lett. 63 (2009) 2396–2398.
[32] Y. Mi, W. Hu, Y. Dan, Y. Liu, Mater. Lett. 62 (2008) 1194–1196.
[33] C.H. Yim, E.A. Baranova, Y. Abu-Lebdeh, I. Davidson, J. Power Sources 205 (2012) 414–419.
[34] C. Chang, J. Xiang, X. Shi, X. Han, L. Yuan, J. Sun, Electrochim. Acta 54 (2008) 623–627.
[35] F. Teng, Z.-H. Hu, X.-H. Ma, L.-C. Zhang, C.-X. Ding, Y. Yu, C.H. Chen, Electrochim. Acta 91 (2013) 43–49.
[36] L. Wang, X. Li, Z. Tang, X. Zhang, Electrochem. Commun. 22 (2012) 73–76.
[37] S. Zhong, L. Wu, J. Liu, Electrochim. Acta 54 (2008) 623–627.